

Research progress of low-dimensional metal halide perovskites for lasing applications

Zhen Liu(刘镇), Chun Li(李淳), Qiu-Yu Shang(尚秋宇), Li-Yun Zhao(赵丽云), Yang-Guang Zhong(钟阳光), Yan Gao(高燕), Wen-Na Du(杜文娜), Yang Mi(米阳), Jie Chen(陈杰), Shuai Zhang(张帅), Xin-Feng Liu(刘新风), Ying-Shuang Fu(英付双), Qing Zhang(张青)

Citation: Chin. Phys. B . 2018, 27(11): 114209. **doi:** 10.1088/1674-1056/27/11/114209

Journal homepage: http://cpb.iphy.ac.cn; http://iopscience.iop.org/cpb

What follows is a list of articles you may be interested in

Fabrication of mixed perovskite organic cation thin films via controllable cation exchange

Yu-Long Zhao(赵宇龙), Jin-Feng Wang(王进峰), Ben-Guang Zhao(赵本广), Chen-Chen Jia(贾晨晨), Jun-Peng Mou(牟俊朋), Lei Zhu(朱磊), Jian Song(宋健), Xiu-Quan Gu(顾修全), Ying-Huai Qiang(强颖怀)

Chin. Phys. B . 2018, 27(2): 024208. **doi:** 10.1088/1674-1056/27/2/024208

Enhanced Kerr nonlinearity in a quantized four-level graphene nanostructure

Ghahraman Solookinejad, M Panahi, E Ahmadi, Seyyed Hossein Asadpour

Chin. Phys. B . 2016, 25(7): 074204. **doi:** 10.1088/1674-1056/25/7/074204

Optical bistability and multistability via double dark resonance in graphene nanostructure

Seyyed Hossein Asadpour, G Solookinejad, M Panahi, E Ahmadi Sangachin

Chin. Phys. B . 2016, 25(6): 064201. **doi:** 10.1088/1674-1056/25/6/064201

Optical bistability and multistability in a defect slab doped by GaAs/AlGaAs multiple quantum wells

Seyyed Hossein Asadpour, G Solookinejad, M Panahi, E Ahmadi Sangachin

Chin. Phys. B . 2016, 25(5): 054208. **doi:** 10.1088/1674-1056/25/5/054208

Influence of Fano interference and incoherent processes on optical bistability in a four-level quantum dot nanostructure

Seyyed Hossein Asadpour, G Solookinejad, M Panahi, E Ahmadi Sangachin

Chin. Phys. B . 2016, 25(3): 034205. **doi:** 10.1088/1674-1056/25/3/034205

TOPICAL REVIEW — Nanolasers

Research progress of low-dimensional metal halide perovskites for lasing applications*

Zhen Liu(刘镇)[1,2], Chun Li(李淳)[1], Qiu-Yu Shang(尚秋宇)[1], Li-Yun Zhao(赵丽云)[1], Yang-Guang Zhong(钟阳光)[1], Yan Gao(高燕)[1], Wen-Na Du(杜文娜)[3], Yang Mi(米阳)[3], Jie Chen(陈杰)[3], Shuai Zhang(张帅)[3], Xin-Feng Liu(刘新风)[3], Ying-Shuang Fu(付英双)[2,†], and Qing Zhang(张青)[1,‡]

[1] *Department of Materials Science and Engineering, College of Engineering, Peking University, Beijing* 100871, *China*
[2] *School of Physics and Wuhan National High Magnetic Field Center, Huazhong University of Science and Technology, Wuhan* 430074, *China*
[3] *Division of Nanophotonics, CAS Key Laboratory of Standardization and Measurement for Nanotechnology, CAS Center for Excellence in Nanoscience, National Center for Nanoscience and Technology, Beijing* 100190, *China*

(Received 1 March 2018; revised manuscript received 4 September 2018; published online 25 October 2018)

Metal halide perovskites have been regarded as remarkable materials for next-generation light-harvesting and light emission devices. Due to their unique optical properties, such as high absorption coefficient, high optical gain, low trapping-state density, and ease of band gap engineering, perovskites promise to be used in lasing devices. In this article, the recent progresses of microlasers based on reduced-dimensional structures including nanoplatelets, nanowires, and quantum dots are reviewed from both fundamental photophysics and device applications. Furthermore, perovskite-based plasmonic nanolasers and polariton lasers are summarized. Perspectives on perovskite-based small lasers are also discussed. This review can serve as an overview and evaluation of state-of-the-art micro/nanolaser science.

Keywords: perovskite, nanostructure, laser, microlaser, emission

PACS: 42.55.Px, 42.55.Sa, 42.55.Tv **DOI:** 10.1088/1674-1056/27/11/114209

1. Introduction

The laser technique has been successfully used for producing high-power, ultra-fast, and small coherent light sources. The term "laser" stems from an acronym for "light amplification by stimulated emission of radiation", which can emit coherent light with a strong intensity and superior directionality through a process of optical amplification based on the stimulated emission of electromagnetic radiation.[1–4] Due to the rapid development of nanoscience and nanotechnology, small solid-state lasers, with physical size comparable to the optical wavelength, have been extensively utilized in a variety of fields, such as high-density data storage, optical integration, and high-resolution bio-imaging. [5,6] Inorganic and organic semiconductor nanostructures in the form of nanowires (NWs) and nanoplatelets (NPs) have been considered as active optical microcavities for achieving lasing over the past three decades.[7] Along with technological innovation, combining gain materials with optical cavities (such as photonic crystals or metal-clad cavities) has been deemed a vital method to realize photonic lasing. For instance, Chen *et al.* successfully realized the single mode, low threshold, and spatially coherent laser operation in the near-infrared region by coupling a semiconductor thin film with photonic crystals.[8] Nevertheless, due to the diffraction limit, the mode and physical dimension of the photonic laser are larger than half of the wavelength of the optical field, which triggers a crucial fundamental challenge to realizing ultra-compact lasers that can directly generate coherent optical fields on a nanometer scale.[9,10] The plasmonic laser, a new class of optical amplification and laser device, has been demonstrated to store electromagnetic field energy in charge density waves.[11,12] A hybrid semiconductor–insulator–metal construction is widely adopted to overcompensate for the losses to realize plasmonic laser, which will be discussed in detail in Section 4.[13] Furthermore, polariton lasers have attracted great attention and play an irreplaceable role in the field of lasing. Unlike photonic and plasmonic lasers, polariton lasers have no threshold condition linked to the inversion of the population and also open up a host of technological possibilities in the applications of slow light, nonlinear optics, and low-threshold coherent emitters.[14,15]

Metal halide perovskites with the general formula ABX_3 or A_2BX_4 are considered as the most promising materials for future optoelectronics. In 2009, Miyasaka *et al.* first used

*Project supported by the National Key Research and Development Program of China (Grant Nos. 2017YFA0304600, 2017YFA0205700, and 2016YFA0200700), the National Natural Science Foundation of China (Grant Nos. 61774003 and 21673054), the Start-up Funding of Peking University, National Young 1000-talents Scholarship of China, the Open Research Fund Program of the State Key Laboratory of Low-Dimensional Quantum Physics, China (Grant No. KF201604), and the Key Research Program of Frontier Sciences, Chinese Academy of Sciences (Grant No. QYZDB-SSW-SYS031).

†Corresponding author. E-mail: q_yfu@hust.edu.cn
‡Corresponding author. E-mail: q_zhang@pku.edu.cn

© 2018 Chinese Physical Society and IOP Publishing Ltd

the $CH_3NH_3PbI_3$ ($MAPbI_3$) as a light absorber in solar cells with an initial efficiency of only 3.8%, Then, due to the improvement of materials and interface engineering, the efficiency was enhanced to over 22%.[16–23] The high absorption coefficient, low nonradiative recombination rate, long diffusion length, low density of defect states, and bipolar carrier-transport property make the perovskites family uniquely suitable for photovoltaic applications.[18,24–26] Besides, owing to the outstanding emission properties such as high photoluminescence (PL) quantum yield (QY) and widely-tuned band gap, perovskites have been extensively utilized in the field of optoelectronic devices, such as in light emitting diodes and photo-detectors.[27–29] Moreover, by virtue of high optical gain, perovskites are regarded as an efficient optical gain medium for lasing applications, including photonic lasing, plasmonic lasing, and polariton lasing. For example, Xing *et al.* first demonstrated the amplification of spontaneous emission (ASE) from a low temperature solution-processed $MAPbX_3$ perovskite thin film in 2014.[30] In addition, through laying $MAPbI_3$ NWs on Ag film with a MgF_2 spacer layer, Yu *et al.* demonstrated Fabry–Pérot (F–P) plasmonic lasers in perovskites.[31] Furthermore, Su *et al.* realized polariton lasing based on all-inorganic cesium lead chloride ($CsPbCl_3$) perovskite NPs at room temperature.[32] In a nutshell, on the basis of the advantages of low-cost fabrication, perovskite microlasers and nanolasers have crucial potential applications in integrated optics. Hence, we will give a general overview about the rapid process of perovskite-based small laser sources. This paper is mainly divided into six parts to review the current research status of perovskite-based small lasers. In Section 2, we will describe the structure and optical property of perovskites. In Section 3, we will review the photonic lasers based on diverged reduced-dimensional perovskites, including NPs, NWs, quantum dots (QDs), and thin films. In Sections 4 and 5, we will briefly discuss the plasmonic laser and polariton laser, respectively. Finally, we will provide a conclusion and give perspectives on future research areas in perovskite small lasers.

2. Crystalline structure and optical properties

2.1. Crystalline structure

On the basis of their crystalline structure, metal halide perovskites can be mainly classified into two categories. The first one is called a three-dimensional (3D) perovskite, with the general chemical formula ABX_3, and the other one is the two-dimensional (2D) or layered perovskite, with the formula A_2BX_4. In terms of a unit cell, A, B, and X are located at the eight corners, the body center, and the six face centers, respectively, as shown in Fig. 1(a). The B is a divalent metal (such as Pb^{2+} or Sn^{2+}), X is a halide (Cl^-, Br^-, or I^-), and A is a cation that can be inorganic (e.g. Cs^+) or organic (e.g. $CH_3NH_3^+$). The atom B is surrounded by six X atoms to form a $[BX_6]$ octahedron, which then constructs a 3D octahedral network. According to the length of the carbon chain, the cation A is either located in the center of an eight $[BX_6]$ octahedral network for the 3D-structured perovskite (middle panel, Fig. 1(a)) or sandwiched between corner-sharing $[BX_6]$ octahedral layers for the 2D-structured perovskite, which is connected by a weak van der Waals force (right panel in Fig. 1(a)).[33–36]

Understanding the underlying mechanism of the energy band structure of perovskites is beneficial to the study of their electron behaviors. Compared with the cation A, the $[BX_6]$ octahedron plays an essential role in constructing a perovskite with a minimum value of the conduction band and a maximum value of the valence band. For instance, through utilizing the density functional theory method, Filippetti *et al.* demonstrated that the minimum value of the conduction band of $MAPbI_3$ is mainly contributed to from p-orbital electrons of Pb atoms and the maximum value of the valence band mainly originates from the s-orbitals of the Pb atoms and the p-orbitals of the I atoms. By contrast, the cation A can only tune the edge band structure via changing the bending and stretching between the Pb and the halogen atoms in the $[PbX_6]$ octahedron.[37,38]

2.2. Optical properties

In the following section, we primarily discuss three optical properties of perovskite essential for the emission devices. (I) Tunable emission. Owing to the ease of band gap engineering, perovskites have been considered as promising candidates for developing the next-generation multicolor coherent and incoherent light sources.[39–43] By changing the stoichiometry, the emission spectrum can be tuned to cover the whole visible range, as shown in Fig. 1(b). The visible fully-covered emission spectrum can be realized by the mixture of chlorides and bromides, or by the mixture of bromides and iodides. The changing of the A cation can further enlarge the emission spectrum into the near infrared or ultraviolet region.[23,30,44–46] (II) High PLQY. PLQY is deemed as the critical characteristic for light emitters, and is defined as the ratio of the number of converted photons to absorbed photons. The quantum efficiency depends on the exciton radiative recombination efficiency, which is beneficial to large exciton oscillator strength and the low density of trapping states. In cesium lead halides and Br-based perovskites, their intrinsic exciton binding energies are quite high, and are further increased in reduced-dimensional structures such as 2D perovskites, and 0D QDs. Therefore, these perovskites are considered as promising alternatives for light-emitting applications.[45,47] (III) Quantum confinement effect. Tailoring the size of the semiconductor to

be comparable to the Bohr radius of excitons can lead to a transition from continuous to discrete energy levels for excitons. For example, in all-inorganic $CsPbBr_3$ perovskite QDs with an exciton Bohr radius of ~ 7 nm, the band gap can be tuned from 2.7 eV to 2.4 eV when the QD diameter varies from 4 nm to 12 nm.[45] This provides an opportunity to tune the optical absorption and emission properties via changing the dimension of the semiconductor, which results in potential applications in various light emissions.[45,47] On account of the strength of above-superior optical properties as well as low-cost fabrication processing, perovskites have been considered as important candidates for the development of the next-generation light sources.

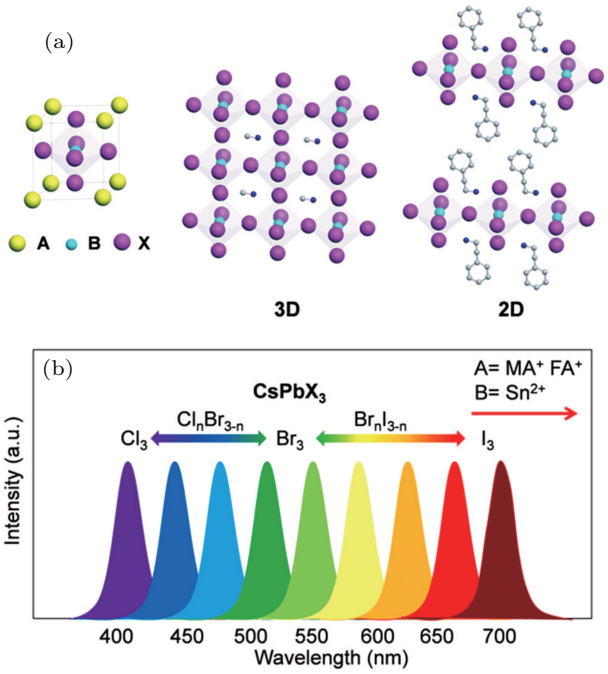


Fig. 1. (color online) (a) Schematic of unit cell and crystalline structure of typical perovskite structures. In a unit cell, A, B, and X are located at eight corners, the body center, and six face centers of the unit cell, respectively (left panel); crystalline structure of ABX_3 (middle panel) and A_2BX_4 (right panel). (b) Wide wavelength tunability of emission color throughout the whole visible region realized by controlling the stoichiometry, such as $A = Cs^+$, $CH_3NH_3^+$, or FA^+, $B = Pb^{2+}$ or Sn^{2+}, and $X = Cl^-$, Br^-, or I^-.

3. Photonic microlasers

3.1. NPs: whispering-gallery mode (WGM) lasers

Currently, high-quality single-crystal perovskites in the form of NPs and microdisks have been demonstrated as excellent WGM microlasers with 2D optical confinement.[48–51] A variety of significant studies have been done in the past few years. In 2014, Zhang *et al.* first realized a room-temperature microlaser based on hybrid organic–inorganic perovskite polygonal $MAPbI_{3-x}(Cl/Br)_x$ NPs, which are derived from a two-step chemical vapor deposition (CVD) route. The schematic diagrams of hexagonal and triangular perovskite NPs and lasing action are shown in Fig. 2(a). For $MAPbI_3$ NPs, the lasing modes are located around 780 nm when the NPs are pumped by a femto-second pulsed laser above the threshold (37 $\mu J \cdot cm^{-2}$) at room temperature. The full width at half maximum (FWHM) of the lasing is ~ 1.2 nm, which indicates a high spectrum coherence. From the perspective of the application, perovskite lasing was also studied when the NPs were integrated with other conductive bases, such as Si, Au, and ITO, to probe the potential of chip-level lasing devices.

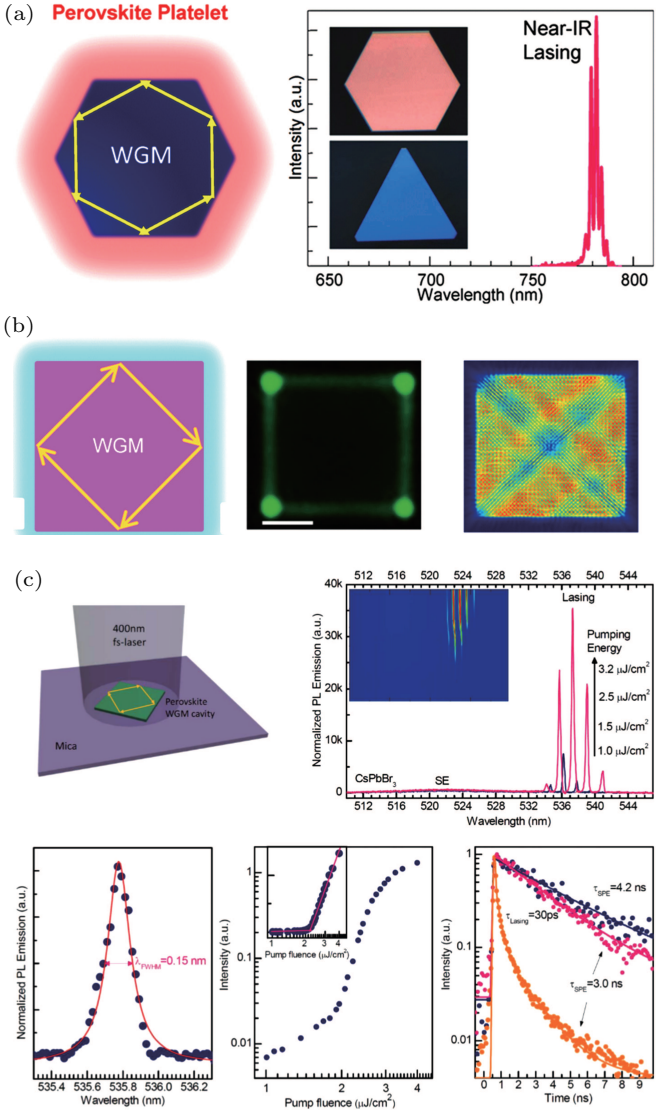


Fig. 2. (color online) (a) Schematic of hexagonal WGM perovskite of $CH_3NH_3PbI_{3-a}X_a$ (X = I, Br, Cl) and the corresponding lasing mode.[52] (b) Schematic of small perovskite lasers based on a WGM cavity with square shape (left panel). The PL emission image from the $CsPbBr_3$ NP above the threshold; the green color shows PL out-coupling from the NP (middle panel). The simulation of the electric field distribution for the square perovskite cavity; the pattern shows that the WGM is supported by the cavity, and the four corners show the stronger out-coupling than that at any other place (right panel).[53] (c) Schematic of a $CsPbX_3$ (X = Cl, Br, or I) NP on mica substrate pumped by 400 nm laser excitation (left panel). Emission spectra with pump fluence increasing from 1.0 $\mu J \cdot cm^{-2}$ to 3.2 $\mu J \cdot cm^{-2}$ (right panel). The FWHM is ~ 0.15 nm and the "S" curve shows a process from spontaneous emission to lasing. After photoexcitation with pump fluence below $P \approx 0.8P_{th}$ and above threshold ($\approx 1.2P_{th}$), TRPL decay kinetics shows an ~ 3.0 ns spontaneous emission decay process and a < 30 ps lasing process, respectively.[53]

Nevertheless, compared with the hybrid organic–inorganic lead halide perovskites, all-inorganic lead halide perovskites exhibit better stability, larger exciton binding energy, and higher emission efficiency.[52] Zhang *et al.* demonstrated the high-quality WGM lasing from cesium lead halide square-shaped perovskite NPs, which were synthesized by the one-step vapor-phase van der Waals epitaxial method on a mica substrate in 2016, as shown in Figs. 2(b) and 2(c).[53] The absorption and PL spectra clearly show a strong excitonic peak with an FWHM of 10–12 nm at room temperature, showing that the large exciton binding energies in all-inorganic perovskites are in a range from 20 meV to 70 meV. For $CsPbBr_3$, with the increase in pump fluence, the input–output curve shows a typical "S" shape, which demonstrates the process from ASE to lasing. The lasing mode FWHM of 0.15 nm and the low threshold of 2.2 $\mu J\cdot cm^{-2}$ are as small as those of previous microlasers (Fig. 2(c)). A multicolor lasing spectrum is achieved by compositional modulation via tuning the ratios of Cl/Br and Br/I.

Considering the further prospects of optoelectronic applications, the arrayed small lasers should be more practical and valuable. Through fabricating patterned lead halide perovskite NPs in periodic arrays on a silicon substrate with micro-patterned BN film as the buffer layer, Liu *et al.* realized room-temperature high-quality WGM lasing with a threshold of ~ 11 $\mu J\cdot cm^{-2}$. By shortening the size of the cavity or breaking the symmetry of the cavity, single mode lasing can be achieved.[54] Meanwhile, by positioning a perovskite NP onto a silicon grating, Wang *et al.* fabricated periodic nanolaser arrays.[55,56] In brief, apart from individual perovskite nanolasers, the development of superior and high-quality integrated perovskite laser arrays may push the preparation of perovskite-based optoelectronic devices into industrial manufacturing.

3.2. NWs: F–P lasers

Compared with other reduced-dimensional structures, NWs are regarded as crucially potential building blocks for future optoelectronic circuits. Semiconductor NWs are perceived as excellent candidates for the realization of miniaturized waveguides and lasers.[57–59] As shown in Fig. 3(a), Zhu *et al.* demonstrated NW lasing on using perovskites in 2015.[60] By adopting a one-step wet-chemical method, a high-quality $MAPbX_3$ perovskite NW Farby–Pérot (F–P) cavity was fabricated, which exhibited an ultra-low lasing threshold of 220 $nJ\cdot cm^{-2}$. Broad tunability covering the region from near-infrared to visible wavelength was also been observed in their work. Such remarkable lasing performance is attributed to the long carrier lifetime and low nonradiative recombination rate in perovskite NWs. When the excitation fluence is below the threshold, the entire NW has a uniform red color; as the excitation fluence exceeds the threshold, two bright spots appear at either end of the NW, indicating the emergence of lasing. Furthermore, Xing *et al.* synthesized perovskite NWs through a two-step vapor-phase synthesis by transferring PbX_2 into $MAPbX_3$ as shown in Fig. 3(b).[61] Under the optical pumping condition, the NWs show near-infrared lasing with a wavelength of 777 nm, a low threshold of 11 $\mu J\cdot cm^{-2}$, and a spectral coherence length of 1.9 nm (laser pulse width: 120 fs). Meanwhile, the lasing behaviors of $MAPbBr_3$ and $MAPbI_xCl_{3-x}$ NWs have been measured,

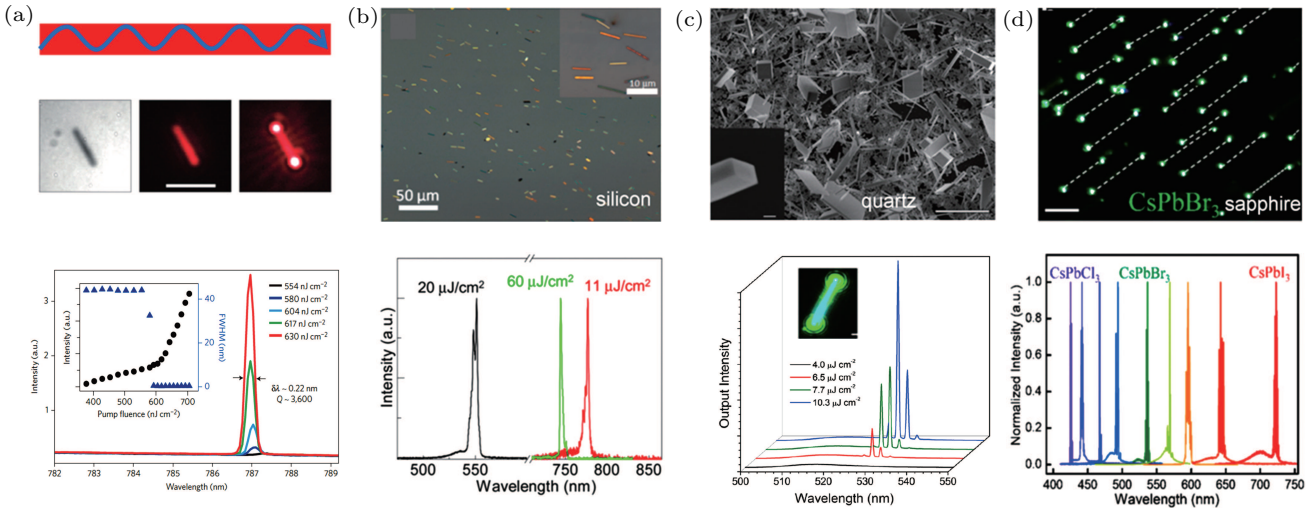


Fig. 3. (color online) (a) Schematic of perovskite NW F–P cavity laser (upper panel); bright-field optical, spontaneous emission, and lasing images of single $CH_3NH_3PbI_3$ NWs (middle panel); lasing spectra of single $CH_3NH_3PbI_3$ NWs (bottom panel).[60] (b) Optical image of $CH_3NH_3PbI_3$ NWs grown on silicon substrate (upper panel) and lasing spectra of $CH_3NH_3PbI_3$, $CH_3NH_3PbBr_3$, and $CH_3NH_3PbI_xCl_{3-x}$ (lower panel).[61] The excitation power is 20 $\mu J\cdot cm^{-2}$, 60 $\mu J\cdot cm^{-2}$, and 11 $\mu J\cdot cm^{-2}$, respectively. (c) SEM images of $CsPbBr_3$ NWs and NPs grown on quartz substrate (upper panel), and power-dependent emission spectra of $CsPbBr_3$ NWs (lower panel).[62] (d) Lasing images of $CsPbBr_3$ NWs directionally grown on sapphire substrate above the lasing threshold (upper panel), and wide range lasing spectra from the directional $CsPbX_3$ and alloy NWs (lower panel).[63]

and the results show that the lasing wavelength (threshold) is 770–744 nm (20 μJ·cm^{-2}) and 551 nm (60 μJ·cm^{-2}) for $MAPbI_xCl_{3-x}$ and $MAPbBr_3$, respectively.[61] Despite the superior lasing performance, the intrinsic poor stability of hybrid perovskite NWs is a problem. Aiming to solve this problem, Eaton *et al.* demonstrated an ultra-stable all-inorganic $CsPbBr_3$ perovskite NW laser working in ambient and vacuum conditions (Fig. 3(c)). After experiencing 109 excitation cycles, the NW laser kept a low threshold of 5 μJ·cm^{-2} and a spectral coherence length of ∼ 0.5 nm, providing abundant proof of the good stability of all-inorganic $CsPbBr_3$ NWs.[62] Moreover, Wang *et al.* demonstrated high-quality in-plane aligned $CsPbX_3$ NWs grown on an annealed M-plane sapphire substrate by the vapor growth method (Fig. 3(d)). Extracted from the input–output curve of $CsPbBr_3$ NW, the lasing threshold and FWHM are 3.6 μJ·cm^{-2} and 0.2 nm, respectively, verifying that the NWs are efficient optical waveguides to achieve high-quality lasers. At the same time, by tuning the chemical stoichiometry, multicolor nanolasers can be achieved at room temperature.[63]

3.3. QD lasers

The semiconductor QD is a type of nanostructure with a size lower than the Bohr radius in three dimensions, and possess a variety of unique optical and electronic properties due to the quantum confinement effect. Based on the superior characteristics of size tunability and structure flexibility, QDs show large optical oscillator strength, high PLQY, and large extinction coefficients, which promise a bright future in flexible display and communication technologies. Recently, perovskite QDs have also attracted more and more attention in the development of incoherent and coherent light sources.[64–67] In 2015, Protesescu *et al.* demonstrated all-inorganic $CsPbX_3$ colloidal QDs synthesized by a one-step reaction between PbX_2 and Cs-oleate in nonpolar solvent. The PL covers all the visible spectrum via compositional control with the FWHM in a range of 12–42 nm, as shown in Fig. 4(a).[45] Exciting the drop-casting $CsPbBr_3$ colloidal solution on a glass substrate, Yakunin *et al.* demonstrated the ASE with a threshold of 5 μJ·cm^{-2} (right panel, Fig. 4(a)).[68] Meanwhile, by using cubic-shaped colloidal $CsPbX_3$ thin films, Wang *et al.* also demonstrated ASE in the visible spectral range in (Fig. 4(b)).[69] Besides, QD structures with different compositions have been coupled with all sorts of cavities, including distributed Bragg reflectors (DBRs), microspheres, and photonic crystals, and their good lasing performances have been demonstrated.[70–72] By the conformal deposition method, Sutherland *et al.* achieved WGM lasing in $MAPbI_3$ perovskite-coated microspheres at 80 K, as shown in Fig. 4(c).[71] On the basis of the *in situ* growth method, Leng *et al.* demonstrated the nonblinking ASE in a QD/SiO_2 core-shell structure with an effective improvement of the moisture resistance and enhanced photostability (Fig. 4(d)).[73] These studies indicate that the perovskite QDs greatly promise flexible lasing devices.

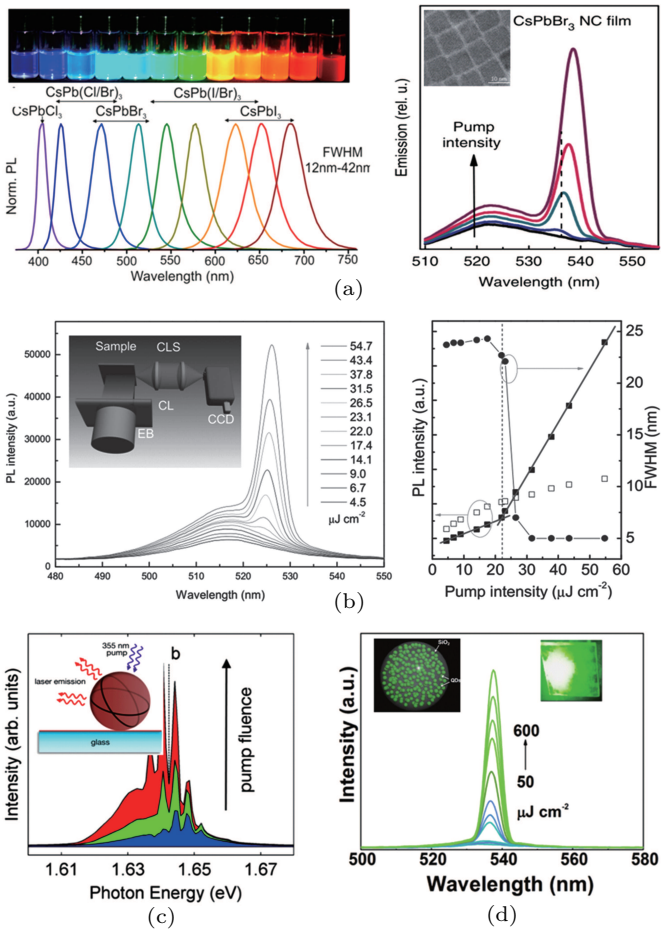


Fig. 4. (color online) (a) Picture of $CsPbX_3$ QD in a solution of toluene, which is excited by an ultraviolet lamp; the corresponding PL spectra are the shown in the bottom (left panel). Pump intensity-dependent PL spectra from $CsPbBr_3$ nanocrystal film (right panel), with inset showing transmission electron microscopy of $CsPbBr_3$ nanocrystals.[45,68,69] (b) Power-dependent PL spectra from a thin film of $CsPbBr_3$ QDs, with the inset showing the fabrication of the device, including the excitation beam (EB), cylindrical lens (CL), collection lens set (CLS), and charged coupled device (CCD) (left panel). The integrated PL intensity and FWHM versus pump intensity exhibits a threshold behavior.[69] (c) Power-dependent $MAPbI_3$ perovskite-coated microsphere emission at 80 K, with the inset showing the device's schematic.[71] (d) Evolution from PL to ASE with increasing pump intensity in a silicon-microsphere resonator embedded with a $CsPbBr_3$ QD.[73]

3.4. Thin film lasers

The cavity-free solution-processed films provide an effective solution to realizing one-chip laser sources integratable into various substrates. Xing *et al.* first illustrated the tunable, robust ASE from $MAPbX_3$ (X = Cl, Br, I, and their mixtures) with a striking low threshold of ∼ 12 μJ·cm^{-2}. By embedding the films into a wide range of cavity resonators, a variety of lasing can be achieved.[74] A photonic crystal is constructed by periodically aligning two media with different dielectric functions, and possesses a widely controllable band gap through

changing the period and dielectric functions (Fig. 5(a)).[75–77] Attributed to this advantage, most industrial laser diodes are fabricated by using DBRs as mirrors, which are typical one-dimensional photonic crystals. Through coupling with the photonic crystal, Chen *et al.* successfully realized a single mode, low threshold, spatially coherent laser operated in the near-infrared region. Besides, by varying the periodic pitch from 430 nm to 460 nm, Nurmikko *et al.* realized single mode lasing tuned in the spectrum range from 768 nm to 795 nm (Fig. 5(b)).[8] By embedding uniform $MAPbI_3$ film into two high-reflectivity DBRs, Chen *et al.* achieved a vertical-cavity surface-emitting laser with a low threshold of 7.6 $\mu J \cdot cm^{-2}$ at room temperature, as shown in Fig. 5(c).[78] Furthermore, Saliba *et al.* achieved low-threshold and tunable distributed feedback lasing via evaporating the perovskite thin film into the photoresist grating structure.[79] Achieving the ultimate goal of electrically pumped laser emission is still a great challenge, but the realization of continuous-wave (CW) optically pumped lasing is widely considered as a vital stepping stone on the path to overcome it. Recently, Jia *et al.* achieved CW lasing in $MAPbI_3$ film, which was deposited on the etched alumina grating on the substrate of sapphire. Figure 5(d) shows the process from spontaneous emission to stimulated emission under CW excitation by the InGaN pump diode at a low temperature of 102 K, and the threshold is about 17 $kW \cdot cm^{-2}$. When the pump fluence increases to above the threshold, a tendency of redshift is clearly observed, and the FWHM is about 0.25 nm at the highest pump intensity.[80] More and more efforts should be encouraged to demonstrate the first CW lasing by using perovskite as a gain medium in low-threshold small lasers. Considering their excellent electric properties, it is very promising to realize chip-level lasing devices based on perovskites.

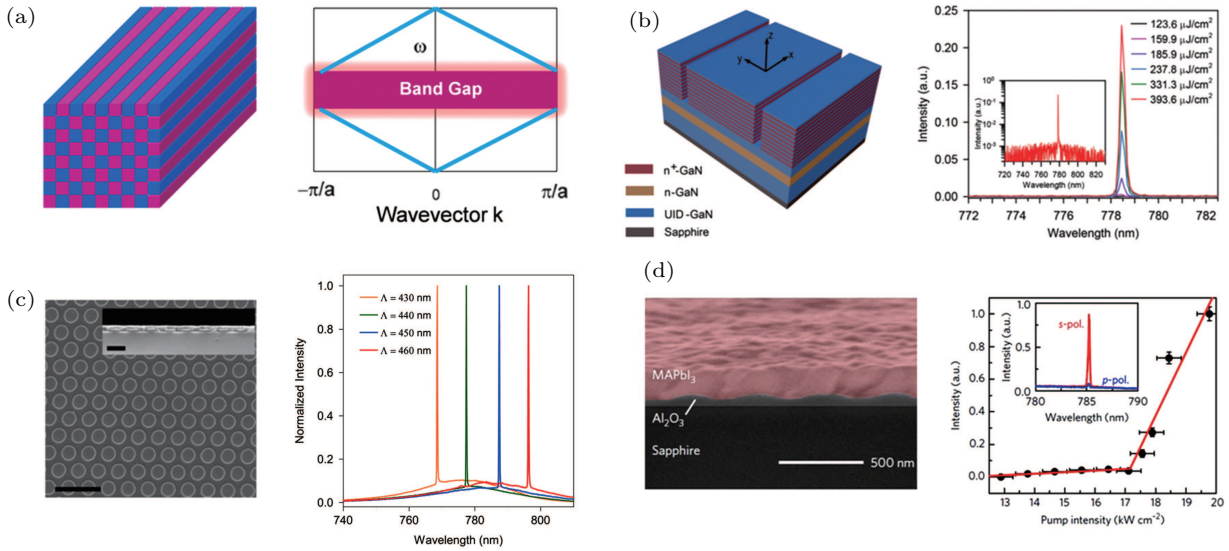


Fig. 5. (color online) (a) Schematic of photonic crystal (left panel), and the band structure of the photonic crystal (right panel). (b) SEM image of 2D photonic crystal nanostructured pattern (left panel), and lasing output from perovskite photonic crystal with the pitch in a range of 430–460 nm. Single mode lasing is observed separately at 768.4 nm, 777.3 nm, 788.1 nm, and 795.8 nm (right panel).[8] (c) Schematic diagram of GaN-based DBRs (left panel), and the single mode lasing spectrum varying with pump fluence at 778.4 nm and FWHM of 0.24 nm.[78] (d) Cross-sectional scanning electron micrograph of the DBR laser architecture, consisting of a $CH_3NH_3PbI_3$ ($MAPbI_3$) film deposited on an 80 nm thick etched alumina grating on a sapphire substrate (left panel), and input–output curve showing the process from spontaneous emission to lasing. The threshold is about 17 $kW \cdot cm^{-2}$, and the inset indicates that the emission spectrum above the threshold is strongly TE-polarized.[80]

4. Plasmon nanolasers

Hindered by the optical diffraction limit, the physical size of a photonic laser is constrained above half of the light wavelength. Nanolaser devices based on the amplification of surface plasmons by stimulated emission of radiation are utilized to push the dimensions of laser devices into the nanometer region beyond the diffraction limit.[11,13,81–86] Oulton *et al.* proposed a hybrid plasmonic waveguide for subwavelength confinement and long-range propagation, which consists of a semiconductor NW separated from a metal surface by a nanoscale dielectric gap. Owing to the continuity of the electric displacement near the dielectric spacer layer, the mode of perovskite NW is confined to an ultra-small mode volume in the dielectric gap region. The coupling between the plasmonic and waveguide modes across the gap makes it possible to store optical energy like a capacitor that allows effective subwavelength transmission in a nonmetallic region with low loss, as shown in Fig. 6(a).[87] On this basis, a deep subwavelength mode confinement of $\lambda^2/400$ to $\lambda^2/40$ can be obtained, and more importantly, surface plasmon polaritons can propagate large distances of 40–150 μm. Based on the structures, plasmonic lasing in the nanometer scale has been realized separately in CdS, GaN, and ZnO NWs.[13,88,89] Recently, Yu *et al.* demonstrated F–P plasmonic lasers based on perovskite NWs.

Figure 6(b) shows a schematic of the plasmonic nanolaser: a single $MAPbI_3$ NW sitting on a Ag film with a 10 nm MgF_2 spacer layer. Figure 6(c) shows the calculated cross-sectional electric field distribution and polarization direction of the hybrid plasmonic mode at the emission wavelength of perovskite (790 nm). The optical feedback is provided by the two end facets of the NW, which can serve as mirrors to form an F–P cavity for forming the plasmon lasing.[31] Compared with the photonic NW laser, where a NW is placed on quartz directly, the plasmonic laser can support optical modes of a free diffraction limit on a nanometer scale where photonic modes cannot even exist. As indicated by the vertical dotted line in Fig. 6(d), the calculated fundamental mode of photonic lasing goes through a cut off point at the diameter of about 146 nm. However, the fundamental mode of hybrid plasmon lasing does not experience any cut off point, which further demonstrates the superiority in this respect. Figure 6(e) shows the plasmonic lasing emission spectra varying with pump power. The Q-factor of the sample here is evaluated to be 151, and the Purcell factor is estimated at 8.3, showing good performance of the lasing characteristics.[31] The research on perovskite plasmonic lasing is still quite limited, and the interaction between perovskite and plasmonic structures is rarely explored. Actually, the underlying photophysics in the new emergent perovskites is not well understood. The hybridization of perovskite and plasmonic structures, i.e. how to use plasmonic structure to tune the exciton properties and therefore reduce the optical losses, is an interesting topic, and more technologies can be generated for lasing applications accordingly.

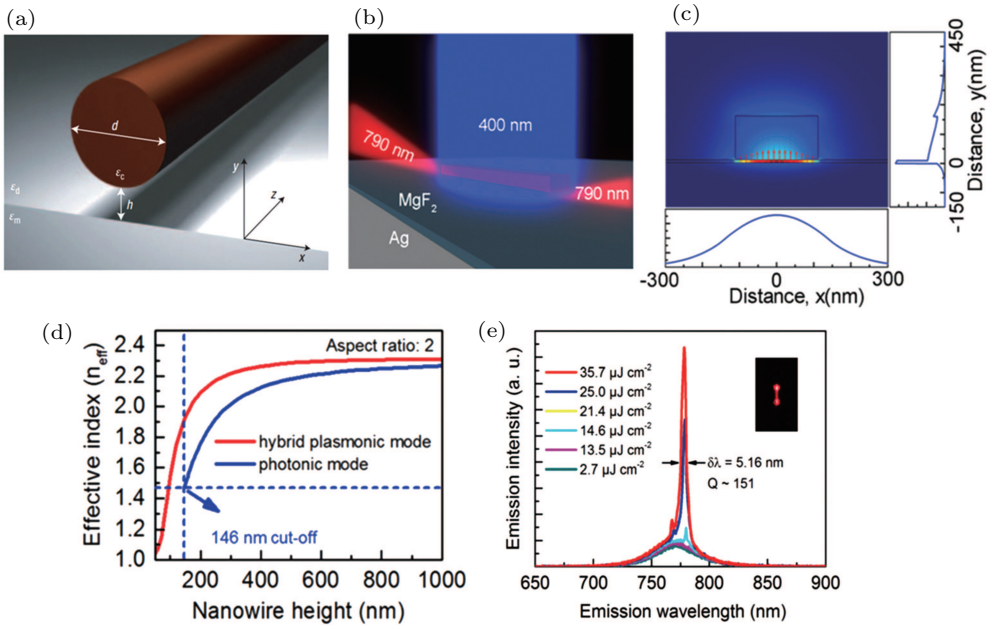


Fig. 6. (color online) F–P NW plasmonic lasers. (a) Hybrid plasmonic waveguide.[87] (b) Schematic of plasmonic nanolaser: a single $CH_3NH_3PbI_3$ ($MAPbI_3$) NW on Ag film with a MgF_2 spacer layer.[31] (c) Calculated NW mode distribution for $MAPbI_3$ NW on Ag film with a 10 nm MgF_2 spacer layer at a wavelength of 790 nm.[31] (d) Calculated effective mode index against NW height for plasmonic and photonic lasing geometry.[31] (e) Emission spectra for different pump intensities, with the inset showing an optical image of the plasmonic lasing NW.[31]

5. Polariton lasers

Comparing with photonic and plasmonic lasing, the concept of polariton lasing was first proposed theoretically in 1996. Unlike photonic lasing accomplished by light amplification through the process of stimulated emission with population inversion, polariton laser based on the Bose–Einstein condensation (BEC) of exciton–polariton is a type of coherent emission without population inversion.[14,32,90–92] In semiconductor microcavities, exciton–polaritons are formed when the interaction time between exciton and polaritons is shorter than their escaping time, which is the so-called strong interaction regime. As shown in Fig. 7(a), the most widely used microcavities for polariton lasing are similar to vertical cavity surface emitting lasing consisting of a planar F–P resonator embedded in two reflectors (usually DBR mirrors) and quantum wells or 2D NPs as the source of excitons. Excitons, as bosons, can couple with cavity photons to form new half-light, half-matter bosonic quasiparticles called polaritons whose effective mass is around 10^4 times less than that of free electrons. According to theoretical analysis, the small effective mass is beneficial to the realization of BEC. Strongly coupled exciton–polaritons then generate the upper polariton branch (UPB) and the lower polariton branch (LPB) in the dispersion relation of energy. Considering that the lifetime of polaritons in the strong coupling regime is extremely short, the whole process cannot reach thermal equilibrium; however the relaxation time is also very short to ensure the final production of

thermalized polariton gas.[90]

Figure 7(b) shows the mechanism of ideal polariton lasing without population inversion.[90] There are two different methods to achieve polariton production: nonresonant excitation at $k_{||} = 0$, and resonant excitation at a larger angle. Under external high-energy excitation, i.e. from an optical pump, a mass of polaritons are created and later fall into the LPB from the UPB through phonon emission. After occupying the exciton-like reservoir in the LPB, polaritons continue to relax mainly by phonon emission until they reach the theoretical value at $k_{||} = 0$. However in this process, phonons with a bigger momentum sharply reduce the probability of emission, causing the relaxation to be not in one step and polaritons to have to "jump down" via losing tiny amounts of energy each time. Due to the fact that phonon–polariton scattering becomes difficult and the lifetime of polaritons decreases close to that of the photon-like final states, the bottleneck effect will occur, which has been observed in several experiments. For further condensation, polariton–polariton scattering is considered as the primary interaction to realize polariton population accumulation in the minimum energy state. Specifically, two polaritons stuck in the bottleneck can exchange energy with each other to make one leap into the area near $k_{||} = 0$, and the other polariton regains a higher momentum. Then, the latter repeats first-stage relaxation once more, eventually inducing polaritons to exclude the bottleneck region as a whole. In the ensuing discussion, we can see, via image analysis, two kinds of scatterings leading to relaxation successively. Finally, the condensate polaritons emit bright coherent light through their photonic component, similar to the scenario of photonic lasing, which can explain the origin of polariton lasing. It is worth mentioning that polariton emission usually shows a continuous blueshift due to the loss of strong coupling under higher pumping or the excitonic part of polaritons under lower pumping, which has been reported in different polariton structures.[14]

In light of the above, strong exciton–photon coupling is the prerequisite for realizing polariton lasing. Over the past two decades, polariton lasing has been demonstrated in inorganic and organic semiconductors. In the earliest research, CdTe, GaAs, and InP have fulfilled potential in polariton condensation below 70 K due to small exciton binding energy. In a subsequent study, room temperature exciton–polariton lasing was achieved in a ZnO- and GaN-microcavity with much higher oscillator strengths and exciton binding energy.[90,93–97] For organic semiconductors, generally speaking, Frankel excitons exhibit larger exciton binding energy but weaker Coulomb interaction, which is against polariton relaxation. In view of the facts presented above, the perovskite system can combine the advantages of both organic and inorganic materials, such as large exciton binding energy, easy fabrication, low trapping states density, and inter-system transition, to achieve high-performance polariton lasing devices.[98–101]

The exciton–polariton has been observed in the system of perovskites, such as $(C_6H_9C_2H_4NH_3)_2PbI_4$, $(C_6H_5C_2H_4NH_3)_2PbI_4$, and $CsPbX_3$. Figure 7(c) shows the conventional energy–wave vector (E–k) dispersion of one $MAPbBr_3$ NW with width × length dimensions of 0.32 μm × 3.66 μm. Meanwhile, the obvious anticrossing feature indicates the occurrence of strong coupling, just like in previous research results. The longitudinal–transverse (L–T) splitting (ΔE_{LT}) is an index of coupling strength, and the L–T splitting energy here is 33 meV, which increases with the decrease in perovskite microcavity size.[15] Another important parameter, the vacuum Rabi splitting energy in $MAPbBr_3$ is ∼ 390 meV, describing a large oscillator strength. Nevertheless, subsequent experiments prove that the lasing here should be photonic lasing rather than polariton lasing. In Fig. 7(d), the lasing peaks are not located in the final state above the threshold, and polariton condensation does not finish, probably due to the low efficiency of relaxation in the bottleneck region. Besides, the continuous blueshift at higher power is almost not visible, suggesting that it is not polariton lasing. Further research remains to be done, and they do offer the possibility of polariton lasing applications in perovskite systems.[15]

Although room temperature, strong exciton–photon coupling in perovskite material has been observed over the past twenty years, the realization of polariton condensation is still a recent breakthrough. In 2017, Su *et al.* first reported polariton lasing in $CsPbCl_3$ NPs at room temperature.[32] The all-inorganic lead chloride perovskites were grown by epitaxial-free CVD and then dry-transferred to a bottom DBR composed of 13 HfO_2/SiO_2 pairs. Through standard e-beam evaporation, seven other pairs were deposited continuously over NPs to form a complete DBR microcavity structure (Fig. 7(e)). The thicknesses of HfO_2 and SiO_2 were precisely designed to support F–P oscillations, and due to the high crystalline quality, the Q-factor of the optical microcavity was estimated to be 300. In order to verify the existence of polariton lasing in the system, the method of different off-resonant excitations was utilized to the probe power-dependent angle-resolved PL spectrum. As the pump fluence increases, the ground state emission intensity at $k_{||} = 0$ shows a transition from a linear region to nonlinear region at the threshold point (P_{th} = 12 μJ·cm^{-2}), the FWHM narrows rapidly, and the intensity increases sharply by more than three orders of magnitude, just like the behaviors in traditional photonic lasing. Under the lower pumping condition, the LPB dispersion exhibits an average emission distribution at all angles, and the emission intensity at $k_{||} = 0$ becomes dramatically stronger than the others corresponding to polariton condensation upon approaching the

threshold fluence. When the excitation power reaches $1.3P_{th}$, almost only the ground state near the minimum of the LPB dispersion is massively occupied, whose energy is ~ 120 meV lower than that of the minimum of the uncoupled cavity mode, indicating the difference between polariton lasing and photonic lasing shown in Fig. 7(f). In the process of polariton condensation, electron–hole pair relaxation is mainly connected with the polariton–reservoir (in fact the excitons in the reservoir) interaction and polariton–polariton interaction. They can lead to two distinct polariton emission energy blueshift trends, which are observed to be consistent with the theoretical results. Meanwhile, polariton condensation emerges clearly.

Finally, we summarize polariton lasing in perovskites. Strong exciton–photon coupling and polariton condensation are the latest concepts, and related studies are still underway. Light–matter interactions in perovskites have been proved constantly, however, in addition to large coupling strength and high polariton density, the realization of a complete relaxation process is also a key points. Devices based on DBR microcavities or NW F–P cavities are feasible, and how to improve the cavity quality will be the next problem for scientists to achieve novel polariton lasing. As a matter of fact, when under higher pumping, polariton lasing can transform into photonic lasing; hence, this also indicates a better future for polariton lasing.

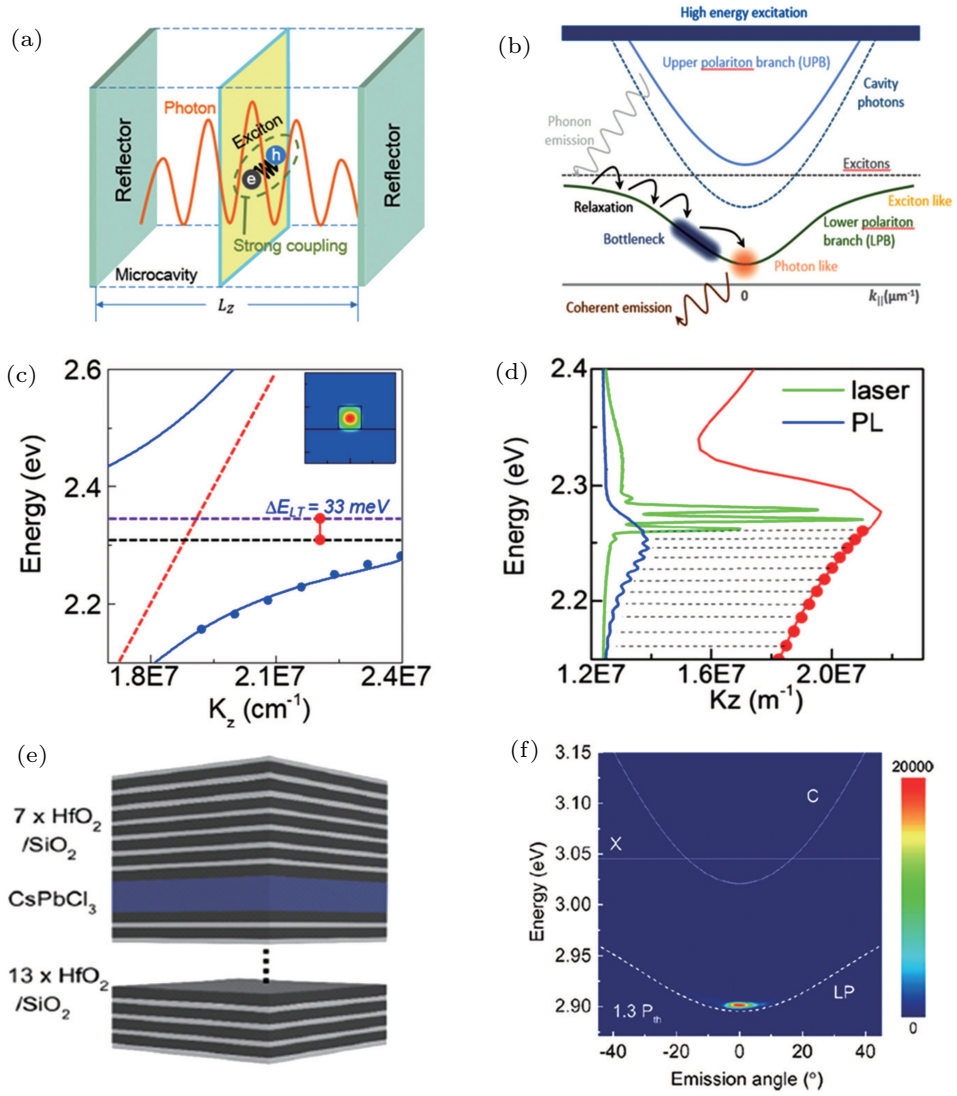


Fig. 7. (color online) Polariton lasing based on perovskites. (a) Microcavity consisting of a planar F–P resonator embedded in two reflectors. Excitons in an active layer and cavity photons can strongly couple with each other to generate new quasiparticles, exciton–polaritons. (b) Mechanism of ideal polariton lasing. Under high-energy excitation, polaritons are created and then leave the UPB for the LPB via phonon emission. Next, they leap down mainly through polariton–phonon scattering before reaching the bottleneck region and through polariton–polariton scattering after reaching the bottleneck to relax continuously to the final state $k_{||} = 0$.[90] (c) Energy–wave vector (E–k) dispersion curves of $CH_3NH_3PbBr_3$ ($MAPbBr_3$) micro/nanowire with a width of 0.32 μm and length of 3.66 μm. The L–T splitting energy (ΔE_{LT}) is about 33 meV, which shows the strong coupling strength. The inset shows a normalized electric field distribution $|E|^2$ at the cross-section of each corresponding wire.[15] (d) Lasing emission spectra (green line) and spatially resolved PL spectra (blue line) of a $MAPbBr_3$ wire in the same condition. The red dots displayed in wave vector space with integer values of π/L_z are F–P peaks extracted from spatially resolved PL spectra, which can be fitted with the polariton dispersion curve (red line).[15] (e) Schematic diagram of the microcavity structure, where $CsPbCl_3$ NPs are embedded in two DBR mirrors consisting of 7 and 13 HfO_2/SiO_2 pairs, respectively.[32] (f) Angle-resolved PL spectrum at high pump fluence of $1.3P_{th}$. Almost all areas around the final state $k_{||} = 0$ are occupied, indicating the realization of the whole polariton condensation.[32]

6. Conclusions and challenges

In this review, we have taken a holistic view to introduce the current status and rapid process of micro-sized and nano-sized lasers based on metal halide perovskites. According to the quantum particles involved in the coherent emission process, lasers are divided into three categories, i.e. photonic lasers, plasmon lasers, and polariton lasers. Due to the excellent properties of high absorption and gain coefficient, low density of trapping states, and tunable emission, metal halide perovskites promise to be used for low-cost, multicolor lasing devices. This is a good opportunity for developing polariton lasing by using perovskite as the gain medium, which is attributed to their large exciton binding energy.

However, challenges still remain. The long-standing problem of poor structural stability due to ionic chemical bonds casts a shadow on practical applications. The 2D structure perovskites exhibit higher stability than their 3D counterparts. The 2D and 3D hybrid structure perovskites provide a solution to the stability issue. Electrical and CW optical pumping is another central challenge to making small perovskite lasers for industrial applications. Although the outstanding electric properties of perovskites have been proven widely in the solar cell research field, small, electrically driven perovskite lasers are rarely explored. The reason for this may lie in the instability of perovskite exposed to air, heat, and organic solvents during the fabrication of microdevices. The high lasing threshold is the other obstacle for electrically driven lasers. Although polariton lasing can reduce the threshold by two–three orders theoretically, the threshold of the as-demonstrated polariton lasers is still quite high. By using $MAPbI_3$, the first CW pumped lasing was developed due to local gain enhancement near the phase transition temperature. However, the underlying physics and universality of the method remain to be confirmed. Interdisciplinary studies on structural engineering, device fabrication, and fundamental photophysics will be helpful for the application of small perovskite lasers.

References

[1] Kim T I, McCall J G, Jung Y H, Huang X, Siuda E R, Li Y, Song J, Song Y M, Pao H A, Kim R H, Lu C, Lee S D, Song I S, Shin G, Al-Hasani R, Kim S, Tan M P, Huang Y, Omenetto F G, Rogers J A and Bruchas M R 2013 *Science* **340** 211

[2] Gather M C and Yun S H 2011 *Nat. Photon.* **5** 406

[3] Miller D A B 2009 *Proc. IEEE* **97** 1166

[4] Smit M, van der Tol J and Hill M 2012 *Laser Photon. Rev.* **6** 1

[5] Johnson J C, Choi H J, Knutsen K P, Schaller R D, Yang P and Saykally R J 2002 *Nat. Mater.* **1** 106

[6] Huang M H, Mao S, Feick H, Yan H, Wu Y, Kind H, Weber E, Russo R and Yang P 2001 *Science* **292** 1897

[7] Zhang Q, Su R, Du W, Liu X, Zhao L, Ha S T and Xiong Q 2017 *Small Methods* **1** 1700163

[8] Chen S, Roh K, Lee J, Chong W K, Lu Y, Mathews N, Sum T C and Nurmikko A 2016 *ACS Nano* **10** 3959

[9] Bergman D J and Stockman M I 2003 *Phys. Rev. Lett.* **90** 027402

[10] Zheludev N I, Prosvirnin S L, Papasimakis N and Fedotov V A 2008 *Nat. Photon.* **2** 351

[11] Hill M T, Marell M, Leong E S P, Smalbrugge B, Zhu Y, Sun M, van Veldhoven P J, Geluk E J, Karouta F, Oei Y S, Nötzel R, Ning C Z and Smit M K 2009 *Opt. Express* **17** 11107

[12] Noginov M A, Zhu G, Belgrave A M, Bakker R, Shalaev V M, Narimanov E E, Stout S, Herz E, Suteewong T and Wiesner U 2009 *Nature* **460** 1110

[13] Oulton R F, Sorger V J, Zentgraf T, Ma R M, Gladden C, Dai L, Bartal G and Zhang X 2009 *Nature* **461** 629

[14] Bajoni D 2012 *J. Phys. D: Appl. Phys.* **45** 313001

[15] Zhang S, Shang Q, Du W, Shi J, Wu Z, Mi Y, Chen J, Liu F, Li Y, Liu M, Zhang Q and Liu X 2018 *Adv. Opt. Mater.* **6** 1701032

[16] Kojima A, Teshima K, Shirai Y and Miyasaka T 2009 *J. Am. Chem. Soc.* **131** 6050

[17] Kim H S, Lee C R, Im J H, Lee K B, Moehl T, Marchioro A, Moon S J, Humphry-Baker R, Yum J H, Moser J E, Grätzel M and Park N G 2012 *Sci. Rep.* **2** 591

[18] Burschka J, Pellet N, Moon S J, Humphry-Baker R, Gao P, Nazeeruddin M K and Gratzel M 2013 *Nature* **499** 316

[19] Jeon N J, Noh J H, Yang W S, Kim Y C, Ryu S, Seo J and Seok S I 2015 *Nature* **517** 476

[20] Lee M M, Teuscher J, Miyasaka T, Murakami T N and Snaith H J 2012 *Science* **338** 643

[21] Liu M, Johnston M B and Snaith H J 2013 *Nature* **501** 395

[22] Saliba M, Orlandi S, Matsui T, Aghazada S, Cavazzini M, Correa-Baena J P, Gao P, Scopelliti R, Mosconi E, Dahmen K H, De Angelis F, Abate A, Hagfeldt A, Pozzi G, Graetzel M and Nazeeruddin M K 2016 *Nat. Energy* **1** 15017

[23] Yang W S 2015 *Science* **348** 1234

[24] Yang W S, Noh J H, Jeon N J, Kim Y C, Ryu S, Seo J and Seok S I 2015 *Science* **348** 1234

[25] Zhou H, Chen Q, Li G, Luo S, Song T-b, Duan H S , Hong Z, You J, Liu Y and Yang Y 2014 *Science* **345** 542

[26] Liu M, Johnston M B and Snaith H J 2013 *Nature* **501** 395

[27] Tan Z K, Moghaddam R S, Lai M L, Docampo P, Higler R, Deschler F, Price M, Sadhanala A, Pazos L M, Credgington D, Hanusch F, Bein T, Snaith H J and Friend R H 2014 *Nat. Nanotechnol.* **9** 687

[28] Li F, Ma C, Wang H, Hu W, Yu W, Sheikh A D and Wu T 2015 *Nat. Commun.* **6** 8238

[29] Cho H, Jeong S H, Park M H, Kim Y H, Wolf C, Lee C L, Heo J H, Sadhanala A, Myoung N and Yoo S 2015 *Science* **350** 1222

[30] Xing G, Mathews N, Lim S S, Yantara N, Liu X, Sabba D, Gratzel M, Mhaisalkar S and Sum T C 2014 *Nat. Mater.* **13** 476

[31] Yu H, Ren K, Wu Q, Wang J, Lin J, Wang Z, Xu J, Oulton R F, Qu S and Jin P 2016 *Nanoscale* **8** 19536

[32] Su R, Diederichs C, Wang J, Liew T C H, Zhao J, Liu S, Xu W, Chen Z and Xiong Q 2017 *Nano Lett.* **17** 3982

[33] Sum T C and Mathews N 2014 *Energy Environ. Sci.* **7** 2518

[34] Sutherl, B R and Sargent E H 2016 *Nat. Photon.* **10** 295

[35] Stranks S D and Snaith H J 2015 *Nat. Nanotechnol.* **10** 391

[36] Byrnes T, Kim N Y and Yamamoto Y 2014 *Nat. Phys.* **10** 803

[37] Filippetti A and Mattoni A 2014 *Phys. Rev. B* **89** 125203

[38] Borriello I, Cantele G and Ninno D 2008 *Phys. Rev. B* **77** 235214

[39] Zhang Q, Ha S T, Liu X, Sum T C and Xiong Q 2014 *Nano Lett.* **14** 5995

[40] Yuan M, Quan L N, Comin R, Walters G, Sabatini R, Voznyy O, Hoogl S, Zhao Y, Beauregard E M, Kanjanaboos P, Lu Z, Kim D H and Sargent E H 2016 *Nat. Nanotechnol.* **11** 872

[41] Zhang X, Lin H, Huang H, Reckmeier C, Zhang Y, Choy W C H and Rogach A L 2016 *Nano Lett.* **16** 1415

[42] Bade S G R, Li J, Shan X, Ling Y, Tian Y, Dilbeck T, Besara T, Geske T, Gao H, Ma B, Hanson K, Siegrist T, Xu C and Yu Z 2016 *ACS Nano* **10** 1795

[43] Liang D, Peng Y, Fu Y, Shearer M J, Zhang J, Zhai J, Zhang Y, Hamers R J, Andrew T L and Jin S 2016 *ACS Nano* **10** 6897

[44] Xing G, Kumar M H, Chong W K, Liu X, Cai Y, Ding H, Asta M, Gratzel M, Mhaisalkar S, Mathews N and Sum T C 2016 *Adv. Mater.* **28** 8191

[45] Protesescu L, Yakunin S, Bodnarchuk M I, Krieg F, Caputo R, Hendon C H, Yang R X, Walsh A and Kovalenko M V 2015 *Nano Lett.* **15** 3692

[46] Hao F, Stoumpos C C, Chang R P H and Kanatzidis M G 2014 *J. Am. Chem. Soc.* **136** 8094

[47] Zhang F, Zhong H, Chen C, Wu X G, Hu X, Huang H, Han J, Zou B and Dong Y 2015 *ACS Nano* **9** 4533

[48] Novoselov K S, Jiang D, Schedin F, Booth T J, Khotkevich V V, Morozov S V and Geim A K 2005 *Proc. Natl. Acad. Sci. USA* **102** 10451

[49] Dean C R, Young A F, Meric I, Lee C, Wang L, Sorgenfrei S, Watanabe K, Taniguchi T, Kim P, Shepard K L and Hone J 2010 *Nat. Nanotechnol.* **5** 722

[50] Xu Z Q , Zhang Y, Lin S, Zheng C, Zhong Y L, Xia X, Li Z, Sophia P J, Fuhrer M S, Cheng Y B and Bao Q 2015 *ACS Nano* **9** 6178

[51] Li L, Yu Y, Ye G J, Ge Q, Ou X, Wu H, Feng D, Chen X H and Zhang Y 2014 *Nat. Nanotechnol.* **9** 372

[52] Zhang Q, Ha S T, Liu X, Sum T C and Xiong Q 2014 *Nano Lett.* **14** 5995

[53] Zhang Q, Su R, Liu X, Xing J, Sum T C and Xiong Q 2016 *Adv. Funct. Mater.* **26** 6238

[54] Liu X, Niu L, Wu C, Cong C, Wang H, Zeng Q, He H, Fu Q, Fu W, Yu T, Jin C, Liu Z and Sum T C 2016 *Adv. Sci.* **3** 1600137

[55] Wang G, Li D, Cheng H C, Li Y, Chen C Y, Yin A, Zhao Z, Lin Z, Wu H, He Q, Ding M, Liu Y, Huang Y and Duan X 2015 *Sci. Adv.* **1** 1500613

[56] Wang K, Gu Z, Liu S, Sun W, Zhang N, Xiao S and Song Q 2016 *J. Phys. Chem. Lett.* **7** 2549

[57] Duan X, Huang Y, Agarwal R and Lieber C M 2003 *Nature* **421** 241

[58] Saxena D, Mokkapati S, Parkinson P, Jiang N, Gao Q, Tan H H and Jagadish C 2013 *Nat. Photon.* **7** 963

[59] Hua B, Motohisa J, Kobayashi Y, Hara S and Fukui T 2009 *Nano Lett.* **9** 112

[60] Zhu H, Fu Y, Meng F, Wu X, Gong Z, Ding Q, Gustafsson M V, Trinh M T, Jin S and Zhu X Y 2015 *Nat. Mater.* **14** 636

[61] Xing J, Liu X F, Zhang Q, Ha S T, Yuan Y W, Shen C, Sum T C and Xiong Q 2015 *Nano Lett.* **15** 4571

[62] Eaton S W, Lai M, Gibson N A, Wong A B, Dou L, Ma J, Wang L W, Leone S R and Yang P 2016 *Proc. Natl. Acad. Sci. USA* **113** 1993

[63] Wang X, Shoaib M, Wang X, Zhang X, He M, Luo Z, Zheng W, Li H, Yang T, Zhu X, Ma L and Pan A 2018 *ACS Nano* **12** 6170

[64] Im J H, Lee C R, Lee J W, Park S W and Park N G 2011 *Nanoscale* **3** 4088

[65] Nozik A J 2009 *Nat. Nanotechnol.* **4** 548

[66] Ning Z, Gong X, Comin R, Walters G, Fan F, Voznyy O, Yassitepe E, Buin A, Hoogl S and Sargent E H 2015 *Nature* **523** 324

[67] Kan S, Mokari T, Rothenberg E and Banin U 2003 *Nat. Mater.* **2** 155

[68] Yakunin S, Protesescu L, Krieg F, Bodnarchuk M I, Nedelcu G, Humer M, De Luca G, Fiebig M, Heiss W and Kovalenko M V 2015 *Nat. Commun.* **6** 8056

[69] Wang Y, Li X, Song J, Xiao L, Zeng H and Sun H 2015 *Adv. Mater.* **27** 7101

[70] Huang C Y , Zou C, Mao C, Corp K L, Yao Y C , Lee Y J , Schlenker C W, Jen A K Y and Lin L Y 2017 *ACS Photon.* **4** 2281

[71] Sutherl B R, Hoogl S, Adachi M M, Wong C T O and Sargent E H 2014 *ACS Nano* **8** 10947

[72] Gong Y, Ellis B, Shambat G, Sarmiento T, Harris J S and Vučković J 2010 *Opt. Express* **18** 8781

[73] Hu Z, Liu Z, Bian Y, Li S, Tang X, Du J, Zang Z, Zhou M, Hu W, Tian Y and Leng Y 2018 *Adv. Opt. Mater.* **6** 1700997

[74] Xing G, Mathews N, Lim S S, Yantara N, Liu X, Sabba D, Grätzel M, Mhaisalkar S and Sum T C 2014 *Nat. Mater.* **13** 476

[75] Yablonovitch E 1987 *Phys. Rev. Lett.* **58** 2059

[76] John S 1987 *Phys. Rev. Lett.* **58** 2486

[77] Sanders J V 1964 *Nature* **204** 1151

[78] Chen S, Zhang C, Lee J, Han J and Nurmikko A 2017 *Adv. Mater.* **29** 1604781

[79] Saliba M, Wood S M, Patel J B, Nayak P K, Huang J, Alexander-Webber J A, Wenger B, Stranks S D, Horantner M T, Wang J T, Nicholas R J, Herz L M, Johnston M B, Morris S M, Snaith H J and Riede M K 2016 *Adv. Mater.* **28** 923

[80] Jia Y, Kerner R A, Grede A J, Rand B P and Giebink N C 2017 *Nat. Photon.* **11** 784

[81] Noginov M A, Zhu G, Belgrave A M, Bakker R, Shalaev V M, Narimanov E E, Stout S, Herz E, Suteewong T and Wiesner U 2009 *Nature* **460** 1110

[82] Kwon S H, Kang J H, Seassal C, Kim S K, Regreny P, Lee Y H, Lieber C M and Park H G 2010 *Nano Lett.* **10** 3679

[83] Ma R M, Oulton R F, Sorger V J, Bartal G and Zhang X 2011 *Nat. Mater.* **10** 110

[84] Flynn R A, Kim C S, Vurgaftman I, Kim M, Meyer J R, Mäkinen A J, Bussmann K, Cheng L, Choa F S and Long J P 2011 *Opt. Express* **19** 8954

[85] Marell M J H, Smalbrugge B, Geluk E J, van Veldhoven P J, Barcones B, Koopmans B, Nötzel R, Smit M K and Hill M T 2011 *Opt. Express* **19** 15109

[86] Lakhani A M, Kim M K, Lau E K and Wu M C 2011 *Opt. Express* **19** 18237

[87] Oulton R F, Sorger V J, Genov D A, Pile D F P and Zhang X 2008 *Nat. Photon.* **2** 496

[88] Lu Y J, Kim J, Chen H Y, Wu C, Dabidian N, Sanders C E, Wang C Y, Lu M Y, Li B H, Qiu X, Chang W H, Chen L J, Shvets G, Shih C K and Gwo S 2012 *Science* **337** 450

[89] Sidiropoulos T P H, Röder R, Geburt S, Hess O, Maier S A, Ronning C and Oulton R F 2014 *Nat. Phys.* **10** 870

[90] Kasprzak J, Richard M, Kundermann S, Baas A, Jeambrun P, Keeling J M, Marchetti F M, Szymanska M H, Andre R, Staehli J L, Savona V, Littlewood P B, Deveaud B and Dang le S 2006 *Nature* **443** 409

[91] Weisbuch C, Nishioka M, Ishikawa A and Arakawa Y 1992 *Phys. Rev. Lett.* **69** 3314

[92] Tredicucci A, Chen Y, Pellegrini V V, Borger M, Sorba L, Beltram F and Bassani F 1995 *Phys. Rev. Lett.* **75** 3906

[93] Dang L S, Heger D, André R, Bœuf F and Romestain R 1998 *Phys. Rev. Lett.* **81** 3920

[94] Lanty G, Zhang S, Lauret J S, Deleporte E, Audebert P, Bouchoule S, Lafosse X, Zuniga-Perez J, Semond F, Lagarde D, Medard F and Leymarie J 2011 *Phys. Rev. B* **84** 195449

[95] Bajoni D, Senellart P, Wertz E, Sagnes I, Miard A, Lemaitre A and Bloch J 2008 *Phys. Rev. Lett.* **100** 047401

[96] Bhattacharya P, Xiao B, Das A, Bhowmick S and Heo J 2013 *Phys. Rev. Lett.* **110** 206403

[97] Christopoulos S, von Hogersthal G B, Grundy A J, Lagoudakis P G, Kavokin A V, Baumberg J J, Christmann G, Butte R, Feltin E, Carlin J F and Grandjean N 2007 *Phys. Rev. Lett.* **98** 126405

[98] Shalabney A, George J, Hutchison J, Pupillo G, Genet C and Ebbesen T W 2015 *Nat. Commun.* **6** 5981

[99] Sanvitto D and Kéna-Cohen S 2016 *Nat. Mater.* **15** 1061

[100] Lanty G, Lauret J S, Deleporte E, Bouchoule S and Lafosse X 2008 *Appl. Phys. Lett.* **93** 081101

[101] Fujita T, Sato Y, Kuitani T and Ishihara T 1998 *Phys. Rev. B* **57** 12428